Eur. Phys. J. D **23**, 43–49 (2003)
DOI: 10.1140/epjd/e2003-00066-0

THE EUROPEAN PHYSICAL JOURNAL D

Compton energy-absorption scattering cross-sections for H, C, N, O, P, Ca and assessment of Doppler broadening

D.V. Rao[1,a], R. Cesareo[1], A. Brunetti[1], and G.E. Gigante[2]

[1] Istituto di Matematica e Fisica, Universita di Sassari, Via Vienna, 2-07100 Sassari, Italy
[2] Dipartimento di Fisica, Universita di Roma "La Sapienza", Ple A. Moro 2, 00185, Roma, Italy

Received 25 June 2002 / Received in final form 27 September 2002
Published online 3rd April 2003 –

Abstract. Total Compton, individual shell and Compton energy-absorption scattering cross-sections are evaluated in the energy region 0.005 to 10 MeV for H, C, N, O, P and Ca. Compton energy absorption cross-sections deviate numerically with available values. The cause of the numerical discrepancies are not fully understood but can be attributed to Doppler broadening of the Compton scattered photons through a given angle.

PACS. 30. Atomic and molecular physics – 32.80.-t Photon interactions with atoms – 32.90.+a Other topics in atomic properties and interactions of atoms with photons

1 Introduction

Incoherent (Compton scattering) is an important mode of photon interaction with atoms and adequately described by the Klein-Nishina theory [1], which assumes target electrons to be initially free and at rest. Although the Klein-Nishina theory gives a satisfactory explanation of this process over most of the region where it is predominant, the incoherent scattering cross-section is found to deviate from its predicted value at low photon energies. This can be understood in terms of the increasing influence of the bound electrons of the scattering medium. An attempt to quantify these deviations have been made under the impulse approximation with the introduction of the so-called incoherent scattering function $S(X, Z)$ as a multiplicative factor to the free electron differential cross-section [2,3].

In dosimetry calculations, use is frequently made of the Compton energy absorption cross-section per electron ($\sigma_{\rm en}$), which expresses the probability of transfer of energy from a photon to an electron by the Compton process. It is equal to the total Compton scattering cross-section per electron ($\sigma_{\rm TC}$) times the fraction (f) of photon energy which is converted to kinetic energy of the recoil electrons in a single collision, averaged over all directions of electron recoil ($\sigma_{\rm en} = \sigma_{\rm TC} f$). Since the range of the recoil electron is small, the Compton energy absorption cross-section per electron is a measure of the total energy communicated locally to the absorbing medium by the Compton process. The most intense Compton scattering is produced in the atomic region $1 \leq Z \leq 20$. For example, most biological and phantom materials of medical interest contain varying proportions of the elements in the above atomic region. It is an attempt to know the effect of Doppler broadening for single atoms, many of which constitute the biological materials. One particular area of interest for these values is in Monte Carlo simulation of photon transport in applications of medical physics [4,5].

It is interesting to estimate these cross-sections by means of double differential scattering cross-sections based on impulse approximation. Impulse approximation refers to large transfers of energy and momentum. However, if the electrons are in motion, as we know to be the case, there is a Doppler effect related to the projected velocities of the electrons. The electron momentum distribution can be determined from the spreading out of the Compton line [6,7]. The motion of the atomic electrons around the atomic nucleus gives rise to Doppler broadening of the apparent energy of the incident photon, resulting in a corresponding broadening of the Compton line for a given deflection angle of the outgoing scattered photon. The shape of this broadened line is called the "Compton profile" and is sensitive to the valancies of the electrons in the atoms and can also give some information about the molecular structure [8].

The impact of Compton profile data [9] on the computation of X-ray cross-section and attenuation coefficients seems not have been explored fully in the literature. The main task of the present work is to examine the Compton profile literature and explore what, if any, effect our knowledge of this line broadening has on theoretical computation of photon incoherent scattering cross-sections and total mass attenuation coefficients. Further, to generate the

[a] e-mail: dvrao@ssmain.uniss.it

tables of total Compton, individual shell and Compton energy absorption cross-sections by means of double differential scattering cross-sections based on impulse approximation with the inclusion of Doppler broadening. This type of new tables are not available in the literature and will be useful for comparison, compilation and simulation purposes for medical and biological applications.

2 Theoretical methods

The Compton's energy shift formula (1) was derived assuming stationary free electrons. It predicts for a given scatter angle θ, a well-defined value of energy of the scattered photon ω_2^c. Detecting the photons at one angle we should measure the same energy for all the photons. In reality, this is not the case. The peak of the energy spectrum of photons scattered at a given angle has an intrinsic width. The reason for the broadening is the initial state of electrons in the atom as a whole. Electrons are not free and not at rest. Each element broadens the energy distribution in its characteristic way. The net result is the breakdown of equation (1) due to its initial electron momentum

$$\omega_2^c = \omega_1[1 + (\omega_1/m_0c^2)(1 - \cos\theta)]^{-1}. \quad (1)$$

The momenta of the bound electrons give rise to a range of possible energies ω_2 for a fixed ω_1 and angle θ, scattering at an angle θ per unit solid angle $\mathrm{d}\Omega'$ for differential energy $\mathrm{d}\omega_2$. An exact evaluation of the double differential scattering cross-section in the relativistic approximation is given by [10]

$$\mathrm{d}^2\sigma/\mathrm{d}\Omega'\mathrm{d}\omega_2 = \frac{(r_0^2/2)m(\omega_2/\omega_1)}{(\omega_1^2 + \omega_2^2 - 2\omega_1\omega_2\cos\theta)^{0.5}}\bar{X}_{KN}J_i(p_z) \quad (2)$$

where r_0 is the classical electron radius, ω_1 and ω_2 are the incident and scattered photon energies for an electron at rest in keV, θ is the scattering angle, $\bar{X}_{KN}$ is the relativistic factor $(\omega_1/\omega_2^c + \omega_2^c/\omega_1 - \sin^2\theta)$, $J_i(p_z)$ is the Compton profile of an electron in the ith sub-shell and p_z is the projection of the recoil electron momentum on the scattering vector, which bisects the incident and scattered photon vectors. The values of p_z, and $\mathrm{d}\omega_2/\mathrm{d}p_z$ are evaluated using the following relations

$$p_z = \omega_1\omega_2(1 - \cos\theta) - \frac{m(\omega_1 - \omega_2)}{(\omega_1^2 + \omega_2^2 - 2\omega_1\omega_2\cos\theta)^{0.5}}$$

$$\mathrm{d}\omega_2/\mathrm{d}p_z = \frac{(\omega_1^2 + \omega_2^2 - 2\omega_1\omega_2\cos\theta)^{0.5}}{m(\omega_2/\omega_1) - \dfrac{p_z(\omega_2 - \omega_1\cos\theta)}{(\omega_1^2 + \omega_2^2 - 2\omega_1\omega_2\cos\theta)^{0.5}}}. \quad (3)$$

Using, $J_i(0)$'s and binding energies [11], the profile function is generated. The Compton profile, $J(p_z)$, in equations (2, 3) takes into account the fact that the electrons in the atom have distribution of velocities. This causes a Doppler shift for the scattered photon. Instead of the single Compton energy, the scattered photons show a broadened spectrum of energies.

The total cross-section is obtained by integrating equation (2) over energy and solid angle intervals and the cross-section for a specific shell is obtained [12]

$$\sigma_i = (\pi r_0^2/\omega_1)\iint \mathrm{d}\theta\mathrm{d}\omega_2(\omega_2|/\mathbf{k} - \mathbf{k}'|) \times (\omega_1/\omega_2^c + \omega_2^c/\omega_1 - \sin^2\theta)J_i(p_z). \quad (4)$$

The limit of the integration in equation (4) for the energy of the scattered photon ω_2 up to $\omega_2 = \omega_1 - I_i$, where I_i is the ionization energy of the electron in the ith shell and ω_2^c is the energy of the Compton scattered photon. The total cross-section is the summation over the occupied shells. The differential form of equation (3) and with $p_z = 0$, further simplifies equation (4)

$$\sigma_i = \pi r_0^2\int_0^\pi \mathrm{d}\theta(\omega_2^c/\omega_1)^2(\omega_1/\omega_2^c + \omega_2^c/\omega_1 - \sin^2\theta)\sin\theta \times \int_{-m}^{p_{i\max}} \mathrm{d}p_z J_i(p_z). \quad (5)$$

The scattering of photons of energy ω_1 by electrons in atoms, molecules, or condensed matter will result in an energy loss $(\omega_1 - \omega_2)$, where ω_2 is the energy of the scattered photon. The energy $(\omega_1 - \omega_2)$ is transferred to the electron (including the binding energy) and the energy absorption cross-section per atom (ignoring emissions of fluorescent photons) may be written as

$$\sigma_{\mathrm{en}} = (1/\omega_1)\iint(1 - g(\omega_1 - \omega_2, Z)) \times (\omega_1 - \omega_2)\mathrm{d}^2\sigma/(\mathrm{d}\Omega'\mathrm{d}\omega_2)\mathrm{d}\Omega'\mathrm{d}\omega_2. \quad (6)$$

The numerical integration of equation (6) with double differential scattering cross-section excluding those electrons for which $(\omega_1 - \omega_2) < E_B$ will give the following simplified expression for the energy absorption per electron and is as follows [13]

$$\begin{aligned}\sigma_{\mathrm{en}} = \pi r_0^2\int_0^\pi \mathrm{d}\theta\sin\theta(\omega_2^c/\omega_1)(1 - \omega_2^c/\omega_1) \\ \times \{\omega_2^c/\omega_1 + \omega_1/\omega_2^c - \sin^2\theta\} \\ \times \sum_i \int_{-\infty}^{p_z(\omega_1 - I_i)} \mathrm{d}p_z J_i(p_z) \\ \times \{1 + \alpha(\omega_1, \omega_2^c, \theta)p_z/m + \beta(\omega_1, \omega_2^c, \theta)(p_z/m)^2\} \\ \times (1 - g(\omega_1 - \omega_2, Z)). \quad (7)\end{aligned}$$

In equations (5, 7) $p_{i\max}$ is the highest p_z value for which an electron in orbital number i is able to be excited. The $p_{i\max}$ is obtained by putting ω_2 up to $\omega_2 = \omega_1 - I_i$, in equation (3), where I_i is the ionization energy of the electron in the ith shell. The $p_{i\max}$ may be positive or negative. The values of α and β are the functions of incident, scattered photon energy and angle. The integration is over

the solid angle $d\Omega'$ and the energy integration is extended to all the shells K, L, M. for electrons in the orbits. In equations (6, 7) $g(\omega_1 - \omega_2, Z)$ is the expectation value of the fraction of the energy transfer $(\omega_1 - \omega_2)$ which is lost due to bremsstrahlung when the liberated secondary electrons (the Compton electron, Auger and Coster-Kronig electrons) are slowed down.

The total double differential scattering cross-section for unpolarised photons for each subshell is evaluated using the following relation

$$d^2\sigma/d\Omega' d\omega' = \sum_i N_i (d^2\sigma/d\Omega' d\omega')_i. \quad (8)$$

Here i denote the sub-shell number and N_i is the number of electrons in the ith shell. However, the summation exclude those electrons for which $(\omega_1 - \omega_2) < E_B$. Energy transfers $(\omega_1 - \omega_2)$ less than the binding energy of the electrons cannot occur. The presence of the absorption edge causes a considerable asymmetry in the energy distribution of the Compton scattered photons, particularly at low incident photon energies.

Two sets of theoretical calculations of total scattering cross-sections are available in literature [13–15]. First set of calculations are derived from double differential scattering cross-sections using impulse approximation [13]. The second set of calculations are derived from differential incoherent scattering cross-section per electron (Klein-Nishina) multiplied by non-relativistic incoherent function, which is a measure of electron binding [14,15].

The later tabulations are based on simplified assumption that the scattered photons are monoenergetic and have energy ω_2^c (Compton energy), *i.e.*, values of σ_{en} are calculated from

$$\sigma_{en} = (1/\omega_1) \int (1 - g(\omega_1 - \omega_2, Z)) \times (\omega_1 - \omega_2^c)(d\sigma_{KN}/d\Omega') S(X, Z) d\Omega' \quad (9)$$

where $(d\sigma_{KN}/d\Omega')$ is the differential incoherent scattering cross-section per electron and $S(X, Z)$ is the incoherent scattering function [$X = \sin(\theta/2)/\lambda, \lambda = 12.3985/\omega_1$, if λ is in units of angstrom and ω_1 in keV].

Total Compton, individual shell scattering cross-sections and Compton energy absorption cross-sections are evaluated using the computer program recently developed by our group [16]. This program generates the data with exclusion of those electrons for which $\omega_1 - \omega_2 < E_B$ in equation (8) by introducing an absorption edge in the double differential cross-section in equation (6). For each incoming photon energy, we have entered the number of shells/sub-shells in atom manually. In this way we entered the binding energy for each shell and also with exclusion of those electrons for which $\omega_1 - \omega_2 < E_B$ and the data is evaluated in the energy region from 0.005 to 10 MeV. The earlier procedure [17] also gave similar results but with considerable amount of time. In addition the incoherent scattering cross-section is sensitive below 5 keV by as much as 20 to 30% with the present formalism.

Table 1. Total Compton scattering cross-sections (b/atom) for H, C, N, O, P, and Ca in the energy region from 0.005 to 10 MeV using the tabulated values of Biggs *et al.* [9].

E (MeV)	H	C	N	O	P	Ca
0.0050	0.5019	2.0584	2.0400	2.6404	3.5473	3.9892
0.0060	0.5409	2.2682	2.6249	2.8507	4.1484	4.7316
0.0080	0.5801	2.5231	2.9519	3.2292	4.8402	5.7857
0.0100	0.6070	2.7325	3.1635	3.5301	5.4027	6.5589
0.0150	0.6241	3.0611	3.5257	3.9031	6.4113	7.8774
0.0200	0.6205	3.2082	3.7379	4.1334	6.9379	8.6512
0.0300	0.6104	3.3078	3.8416	4.3045	7.4727	9.4552
0.0400	0.5916	3.2841	3.8278	4.3077	7.6361	9.7485
0.0500	0.5735	3.2269	3.7576	4.2496	7.6421	9.8197
0.0600	0.5561	3.1550	3.6761	4.167	7.5684	9.7870
0.0800	0.5243	2.9991	3.4993	3.9736	7.3115	9.5249
0.1000	0.4959	2.8509	3.3225	3.7825	7.0108	9.1661
0.1500	0.4371	2.5259	2.9451	3.3568	6.2755	8.2566
0.2000	0.3916	2.2665	2.6425	3.0148	5.6539	7.4620
0.3000	0.3250	1.8850	2.1986	2.5094	4.6213	6.2399
0.4000	0.2793	1.6188	1.8887	2.1557	4.0586	5.3754
0.5000	0.2451	1.4215	1.6586	1.8937	3.5676	4.7248
0.6000	0.2188	1.2704	1.4816	1.6924	3.1878	4.2260
0.8000	0.1812	1.0524	1.2277	1.4015	2.642	3.5036
1.0000	0.1547	0.9002	1.0503	1.1997	2.2616	2.9981
1.5000	0.1151	0.6681	0.7795	0.8903	1.6787	2.2280
2.0000	0.0921	0.5343	0.6233	0.712	1.3428	1.7806
3.0000	0.0665	0.3854	0.4496	0.513	0.9681	1.2853
4.0000	0.0517	0.3013	0.3515	0.4017	0.7592	1.0054
5.0000	0.0434	0.2515	0.2922	0.3331	0.6283	0.8342
6.0000	0.0364	0.2121	0.2474	0.2828	0.5338	0.7068
8.0000	0.0284	0.1648	0.1922	0.2192	0.4142	0.5494
10.0000	0.0234	0.1351	0.1576	0.1797	0.339	0.4503

3 Results and discussion

Relativistic double differential scattering cross-sections for H, C, N, O, P and Ca are evaluated using the tabulated data of $J_i(p_z)$ [9] for a limited energy region. The required $J_i(p_z)$ are interpolated from the aforementioned tables. The relativistic double differential scattering cross-sections are confined to a whole atom. Total Compton scattering cross-sections and Compton energy absorption cross-sections for H, C, N, O, P and Ca are obtained in the energy region from 0.005 to 10 MeV through integration of the double differential cross-section over energy. The Total Compton scattering cross-sections evaluated using equation (5) are presented in Table 1.

The derived total scattering cross-sections will reflect on the current knowledge of the tabulations of total cross-sections estimated using equations (4, 5). The tabulation based on equations (6, 7) will be used only to select the energy of the scattered photon. The total cross-sections based on equation (9) will be used for each scattering angle. It is interesting to note that the incoherent scattering function $S(X, Z)$ increases monotonically with increasing momentum transfer, approaching Z, as $X \to \infty$. At high photon energies $(\lambda \to 0, X \to \infty)$ the scattering approaches that against free electron at rest $(d\sigma_{KN}/d\Omega')$ Z being the free electron differential scattering cross-section per atom. For a given value of Z, the deviation of $S(X, Z)$ from its upper limit Z increases with increasing atomic number, *i.e.*, with higher binding energies of the atomic

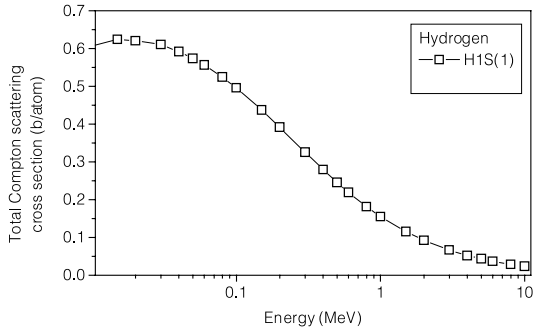

Fig. 1. Total Compton scattering cross-section in the energy region from 0.005 to 10 MeV for hydrogen.

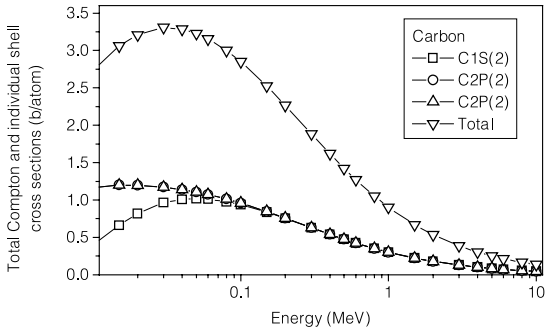

Fig. 2. Total Compton and individual shell cross-sections in the energy region from 0.005 to 10 MeV for carbon.

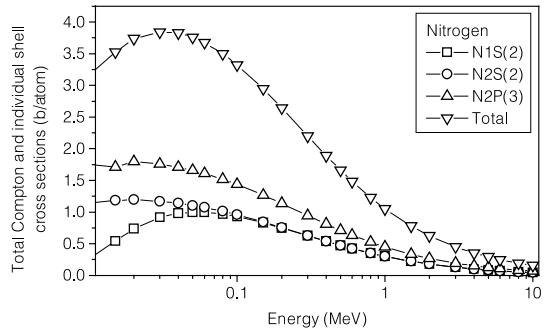

Fig. 3. Total Compton and individual shell cross-sections in the energy region from 0.005 to 10 MeV for nitrogen.

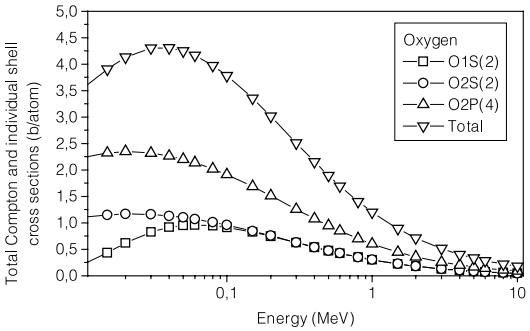

Fig. 4. Total Compton and individual shell cross-sections in the energy region from 0.005 to 10 MeV for oxygen.

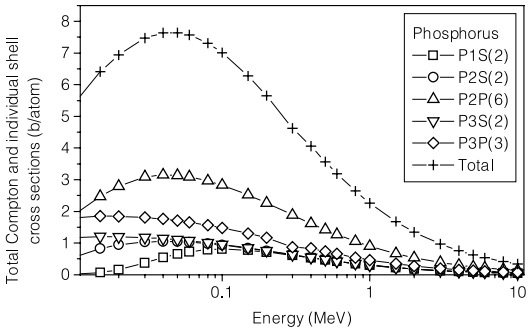

Fig. 5. Total Compton and individual shell cross-sections in the energy region from 0.005 to 10 MeV for phosphorus.

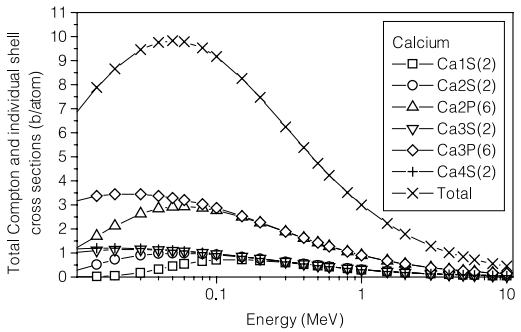

Fig. 6. Total Compton and individual shell cross-sections in the energy region from 0.005 to 10 MeV for calcium.

electrons. However, in cases where the energy transferred to the electron in the scattering process is much larger than the binding energy of the electron, the differential incoherent scattering cross-section ($\mathrm{d}\sigma_{KN}/\mathrm{d}\Omega'$) per electron can be used.

Total Compton and individual shell scattering cross-sections evaluated using equations (4, 5) in the energy region from 0.005 to 10 MeV are shown in Figures 1–6. Figures 7–12 show the comparison of the scattering cross-section data [9,18,19] in the energy region 0.005 to 10 MeV. Figures 13–18 shows the comparison of the ratios [9,18,19]. Figure 19 shows the comparison of the present Compton energy absorption cross-sections with theoretical estimates (Fig. 19) and the ratios (Fig. 20) in the energy region from 0.005 to 10 MeV for H, C, N, O, P and Ca. These figures support the transition to free electron behavior at high energies. Figures 21–25 show the atomic number dependence for few representative energies. The energy broadening of the scattered photons from these materials reflects the momentum distribution of the target electrons. The results are compared with theoretical estimates calculated using Compton profile compilations [9], since the difference between the calculations published so far [18,19] are below 1%. The cause of the numerical discrepancies are not fully understood but can be attributed to Doppler broadening. However, the cause of the significant differences at low energies can be explained in the following way. At low energies, the least tightly bound sub-shells provide most of the cross-section. This is the result of the fact that the energy transfer must be high enough to overcome the electron binding in order to ionize. The sub-shell with most tightly bound electrons,

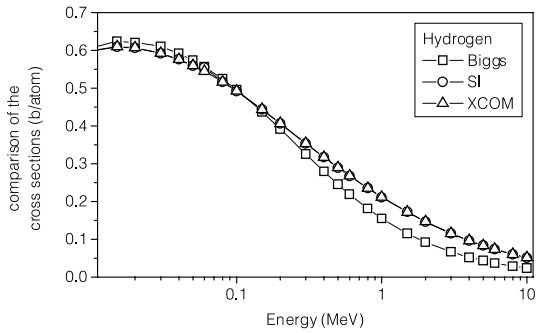

Fig. 7. Comparison of the cross-sections obtained using reference [9] with references [18,19] in the energy region from 0.005 to 10 MeV for hydrogen.

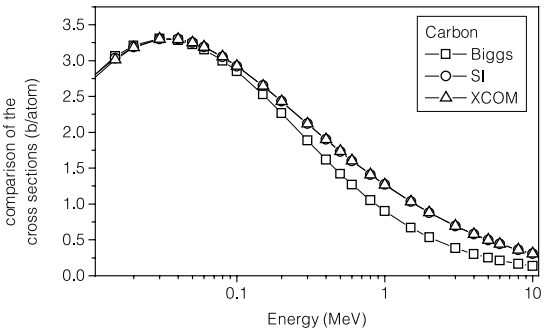

Fig. 8. Comparison of the cross-sections obtained using reference [9] with references [18,19] in the energy region from 0.005 to 10 MeV for carbon.

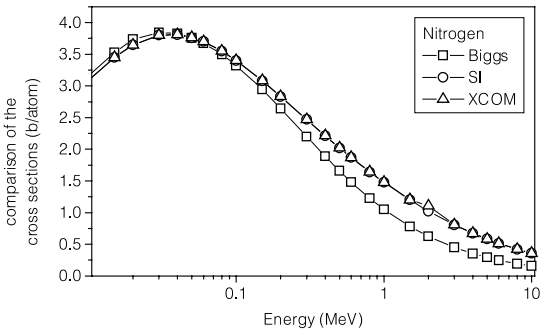

Fig. 9. Comparison of the cross-sections obtained using reference [9] with references [18,19] in the energy region from 0.005 to 10 MeV for nitrogen.

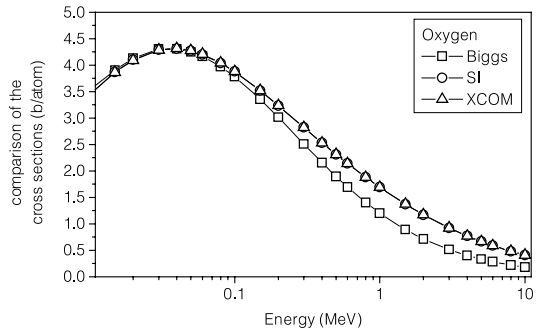

Fig. 10. Comparison of the cross-sections obtained using reference [9] with references [18,19] in the energy region from 0.005 to 10 MeV for oxygen.

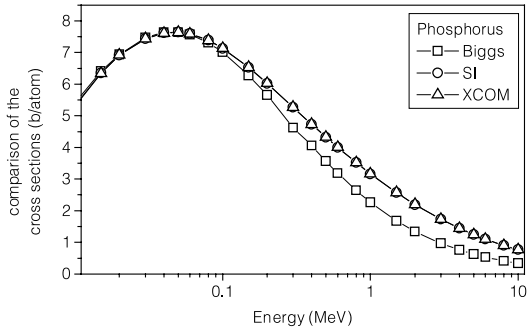

Fig. 11. Comparison of the cross-sections obtained using reference [9] with references [18,19] in the energy region from 0.005 to 10 MeV for phosphorus.

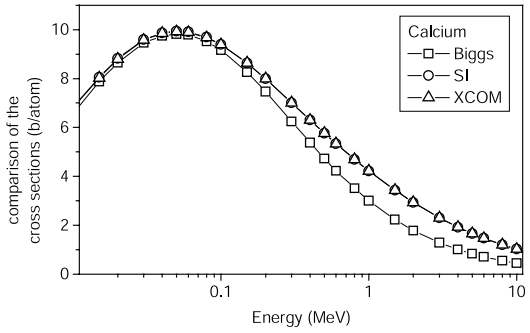

Fig. 12. Comparison of the cross-sections obtained using reference [9] with references [18,19] in the energy region from 0.005 to 10 MeV for calcium.

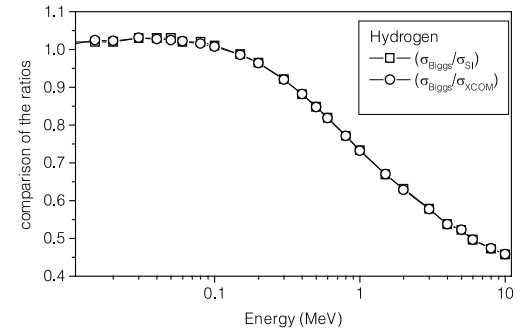

Fig. 13. Comparison of the cross-section ratios with cross-sections obtained from reference [9] with cross-sections from references [18,19] for hydrogen.

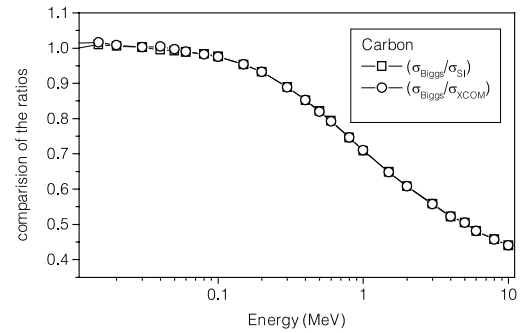

Fig. 14. Comparison of the cross-section ratios with cross-sections obtained from reference [9] with cross-sections from references [18,19] for carbon.

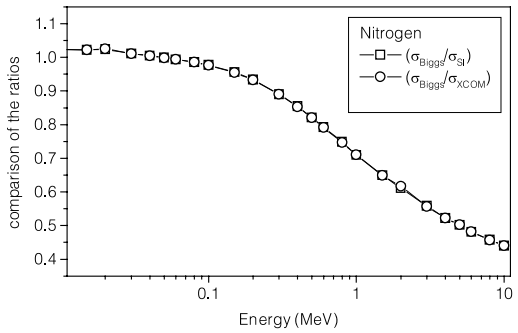

Fig. 15. Comparison of the cross-section ratios with cross-sections obtained from reference [9] with cross-sections from references [18,19] for nitrogen.

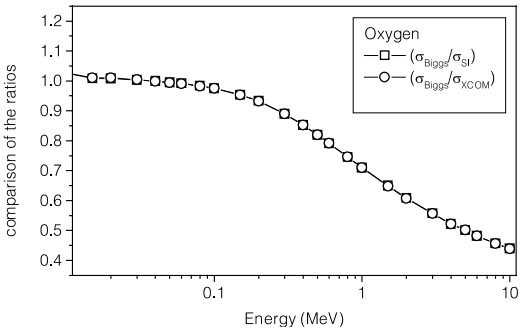

Fig. 16. Comparison of the cross-section ratios with cross-sections obtained from reference [9] with cross-sections from references [18,19] for oxygen.

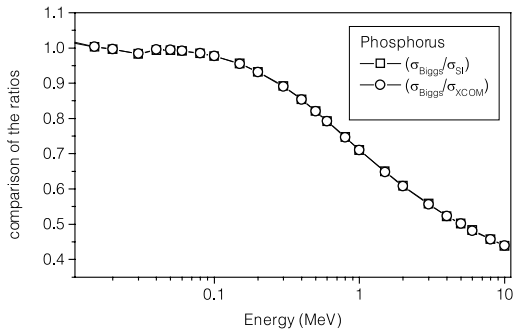

Fig. 17. Comparison of the cross-section ratios with cross-sections obtained from reference [9] with cross-sections from references [18,19] for phosphorus.

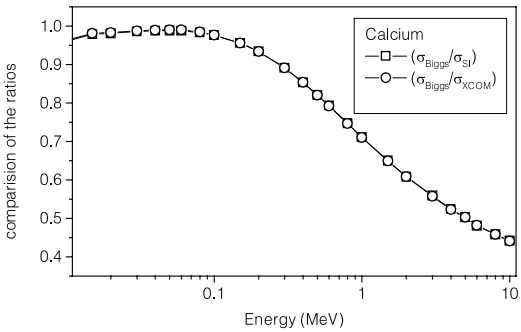

Fig. 18. Comparison of the cross-section ratios with cross-sections obtained from reference [9] with cross-sections from references [18,19] for calcium.

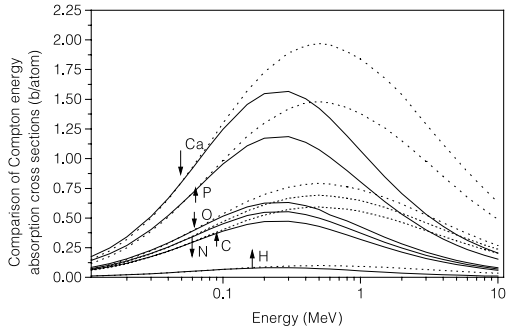

Fig. 19. Comparison of the Compton energy absorption cross-sections obtained using the tabulated profile values of reference [9] (continuous curve) with cross-sections from reference [19] (dashed curve) in the energy region from 0.005 to 10 MeV for hydrogen, carbon, nitrogen, oxygen, phosphorus and calcium.

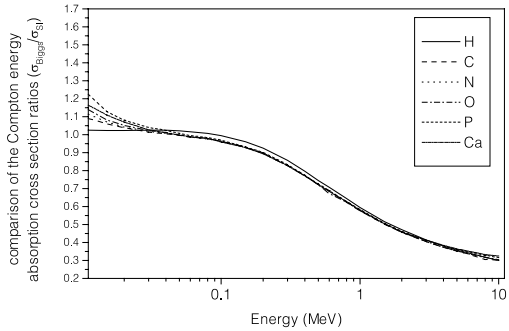

Fig. 20. Comparison of the cross-section ratios of Figure 19 in the energy region from 0.005 to 10 MeV for hydrogen, carbon, nitrogen, oxygen, phosphorus and calcium.

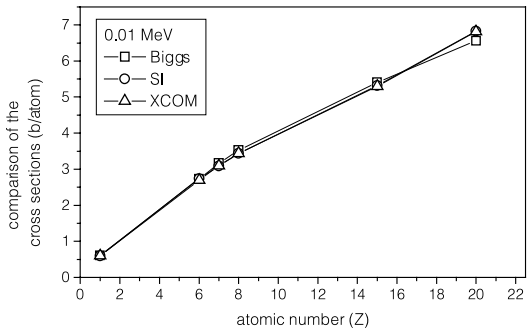

Fig. 21. Variation of the cross-section with atomic number (Z) at 0.01 MeV.

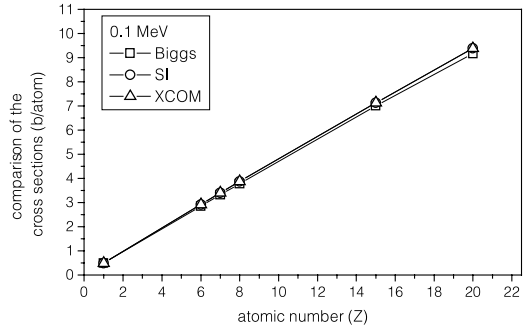

Fig. 22. Variation of the cross-section with atomic number (Z) at 0.1 MeV.

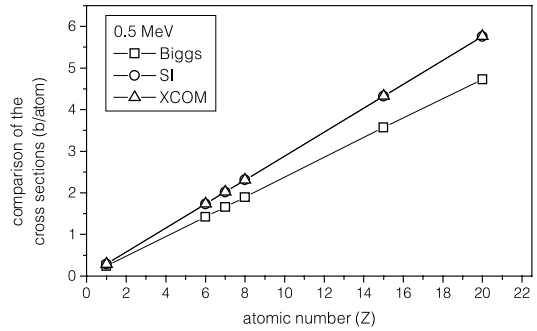

Fig. 23. Variation of the cross-section with atomic number (Z) at 0.5 MeV.

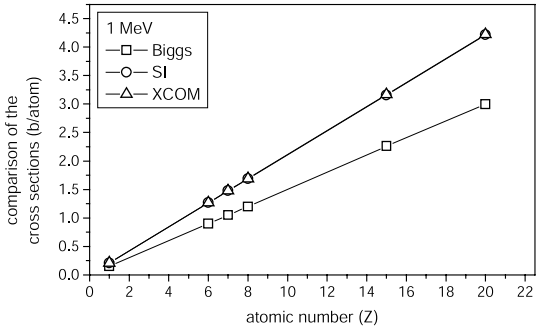

Fig. 24. Variation of the cross-section with atomic number (Z) at 1 MeV.

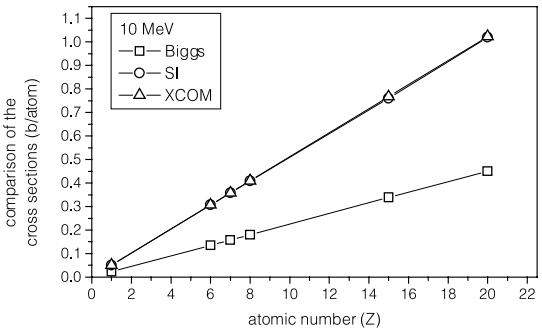

Fig. 25. Variation of the cross-section with atomic number (Z) at 10 MeV.

therefore is the last one to overcome electron binding and contribute completely to the total cross-section. At higher energies, each electron contributes equally to the over all cross-sections and the sub-shell ratios are determined by the number of electrons in the given sub-shell. It is interesting that this transition to free electron behavior doesn't happen until fairly high energies, almost 500 keV for calcium.

4 Conclusion

The present results will give an orderly impression of the magnitude of the Doppler broadening and reflects on the current knowledge. However, extensive tables derived using this formalism and comparison with available tables may provide some new information about the influence of Doppler broadening.

One of the authors (DVR) carried out part of this work with a financial support from ICTP, Trieste, Italy, and would be very grateful to Prof. Dr. G. Furlan, ICTP, Trieste, Italy, for continuous encouragement and help through out the study.

References

1. O. Klein, Y. Nishina, Z. Phys. **52**, 853 (1929)
2. V.V. Rao, D.V. Rao, Phys. Rev. A **28**, 1527 (1983)
3. R. Cesareo, A.L. Hanson, G.E. Gigante, L.J. Pedraza, S.Q.G. Mahtaboally, Phys. Rep. **213**, 117 (1992)
4. J.H. Hubbell, Phys. Med. Biol. **44**, R1 (1999)
5. S.M. Seltzer, Rad. Res. **136**, 147 (1993)
6. J.W.M. DuMond, Phys. Rev. **33**, 643 (1929)
7. J.W.M. DuMond, Phys. Rev. **36**, 146 (1930)
8. J.W.M. DuMond, Rev. Mod. Phys. **51**, 1 (1933)
9. F. Biggs, L.B. Mendelsohn, J.B. Mann, At. Data. Nucl. Data. Tab. **16**, 201 (1975)
10. R. Ribberfors, K.F. Berggren, Phys. Rev. A **26**, 3325 (1982)
11. J.A. Bearden, A.F. Burr, Rev. Mod. Phys. **39**, 125 (1975)
12. G.A. Carlsson, C.A. Carlsson, K.-F. Berggren, R. Ribberfors, Med. Phys. **9**, 868 (1982)
13. R. Ribberfors, Phys. Rev. **27**, 3061 (1983)
14. J.H. Hubbell, Rad. Res. **70**, 58 (1977)
15. J.H. Hubbell, Wm.J. Veigele, E.A. Briggs, R.T. Brown, D.T. Cromer, R.J. Howerton, J. Phys. Chem. Ref. Data. **4**, 471 (1975); erratum in **6**, 615 (1977)
16. A. Brunetti, R. Cesareo, D.V. Rao, Internal report, Istituto di Matematica e Fisica, Universita di Sassari, Italy, 2002
17. D.V. Rao, Doppler broadening calculations of Compton scattering, Computational Radiation Dosimetry: New Applications and Needs for Standards and Data (invited), April 7, 2000, NIST, Gaithersburg, MD, USA (2000)
18. M.J. Berger, J.H. Hubbell, XCOM, NBSIR 87-3597, 1987
19. E. Storm, H.I. Israel, Nucl. Data Tab. A **7**, 565 (1970)